Multiscale Deterministic Wave Modeling with Wind Input and Wave Breaking Dissipation

Lian Shen
Department of Civil Engineering
Johns Hopkins University
Baltimore, MD 21218
phone: (410) 516-5033 fax: (410) 516-7473 email: LianShen@jhu.edu

Award Number: N00014-06-1-0658

LONG-TERM GOAL

The primary focus of this research is to use large-eddy simulation (LES) and large-wave simulation (LWS) to obtain improved physical understanding of wind-wave-ocean interactions, based on which we aim to develop effective models of wind input and whitecapping dissipation for phase-resolving, nonlinear wave-field simulation at large scales. Our ultimate goal is to establish a numerical capability for predicting deterministically large-scale nonlinear wave-field in real marine environments with the presence of significant wind and wave breaking effects.

OBJECTIVES

The scientific and technical objectives of this research are to:

- develop advanced LES and LWS numerical capabilities for wind-wave-ocean interactions with physics-based subgrid-scale (SGS) models; use high-performance LES/LWS as a powerful research tool to obtain an improved understanding of the flow structure in the atmosphere-ocean wave boundary layer

- develop effective models for wind input and the associated whitecapping dissipation in a direct phase-resolving context, which can be readily incorporated into the deterministic numerical tool of the Simulation of Nonlinear Ocean Wave-field (SNOW)

- understand effects of multi-scale physics and environmental uncertainties upon wave deterministic propagation, and to effectively model these effects; validate the direct modeling and simulation approach, and perform direct comparison with existing theories and field measurements

APPROACH

We use a systematic, multiscale approach to investigate and to model effects of wind input and whitecapping dissipation on wave-field evolution. This includes: (1) use LES and LWS to obtain improved physical understanding of wind-wave-ocean interactions at small scales (O(1~10) significant gravity wave lengths); (2) based on the LES/LWS results, develop advanced wind input and

Report Documentation Page

Form Approved
OMB No. 0704-0188

1. REPORT DATE	2. REPORT TYPE	3. DATES COVERED
2009		**00-00-2009 to 00-00-2009**

4. TITLE AND SUBTITLE	5a. CONTRACT NUMBER
Multiscale Deterministic Wave Modeling with Wind Input and Wave Breaking Dissipation	5b. GRANT NUMBER
	5c. PROGRAM ELEMENT NUMBER
6. AUTHOR(S)	5d. PROJECT NUMBER
	5e. TASK NUMBER
	5f. WORK UNIT NUMBER
7. PERFORMING ORGANIZATION NAME(S) AND ADDRESS(ES) **Johns Hopkins University,Department of Civil Engineering,Baltimore,MD,21218**	8. PERFORMING ORGANIZATION REPORT NUMBER
9. SPONSORING/MONITORING AGENCY NAME(S) AND ADDRESS(ES)	10. SPONSOR/MONITOR'S ACRONYM(S)
	11. SPONSOR/MONITOR'S REPORT NUMBER(S)

12. DISTRIBUTION/AVAILABILITY STATEMENT
Approved for public release; distribution unlimited

13. SUPPLEMENTARY NOTES

14. ABSTRACT

15. SUBJECT TERMS

16. SECURITY CLASSIFICATION OF:			17. LIMITATION OF ABSTRACT	18. NUMBER OF PAGES	19a. NAME OF RESPONSIBLE PERSON
a. REPORT **unclassified**	b. ABSTRACT **unclassified**	c. THIS PAGE **unclassified**	**Same as Report (SAR)**	**12**	

whitecapping models in a direct physical context in terms of surface pressure distribution and flow field filtering, respectively; and (3) incorporate the models into SNOW simulation to investigate local effects of wind forcing and whitecapping on large-scale wave-field evolution. Because the physics are being investigated and modeled in a direct, phase-resolving context, we expect that the models developed in this study are more likely to succeed than traditional phase-averaged parameterizations.

The numerical study of wind-ocean-wave interactions are at two fronts: viscous flow simulation for turbulence-wave interactions at small scales, and potential flow based wave simulation at large scales. For viscous air-wave-water simulations, we use the approach of large-eddy simulation based on filtered Navier-Stokes equations, in which large turbulence eddies are computed explicitly with effects of small eddies being represented by SGS models. A similar LWS approach is used for wave-turbulence interactions, with large wave components being simulated directly and small wave effects modeled.

One of the major issues with simulating coupled air-wave-water turbulent flows is the presence of a deformable, time-evolving free surface, which makes the air and water computational domains irregular. The location and geometry of the free surface are unknown beforehand, and they are part of the solution to be solved for. To overcome this difficulty, we have developed a suite of complementary computational methods, which include a boundary interface tracking method based on boundary-fitted grids for moderate wave slope and an Eulerian interface capturing method based on a level set approach for steep/breaking waves.

The wind input and whitecapping models developed from LES/LWS study will be incorporated to potential flow wave computation using SNOW developed at MIT. The SNOW uses a high-order spectral (HOS) method, which is a pseudo-spectral method developed based on the Zakharov equation and mode-coupling idea. The wind input to the wave-field is modeled by surface distribution of pressure, while wave breaking dissipation is represented by advanced filtering treatment in physical and spectral spaces.

The multiscale modeling of ocean wave-fields will be one of the foci of this research. At local scales, we apply LES and LWS, with which the large eddies and waves are resolved explicitly and structures smaller than the computational grid are modeled. The wind input and models developed based on local-scale LES/LWS are then implemented in SNOW for large-scale simulations. In SNOW, the nonlinear wave interactions, the wind input, and the whitecapping dissipation are all represented in a direct physical context. This approach provides a powerful tool and a unique opportunity to investigate the effects of local processes on large-scale wave-field evolution in a physical-based, deterministic way.

Large-scale high-performance computation on parallel computers is used to meet the computational challenges in the turbulence and wave simulations. Massage passing interface (MPI) based on domain decomposition is used for parallelization.

WORK COMPLETED

During the fiscal year of 2009, substantial progresses have been made, which include:

- We have validated our simulation results through extensive comparison with measurement and simulation data in the literature.
- We have quantified and characterized wind input to nonlinear irregular wavefield that evolves dynamically under wind action in the simulation.
- We have analyzed the pressure variation near the wave surface, the result of which is helpful for field measurement of wind input to waves.
- We have extended the simulation capability to turbulence transport of scalars in marine atmospheric boundary layer.
- We have performed direct simulation of steep and breaking wind-waves and airflow separation, and quantified the associated wind-wave interaction processes.
- We have extended the simulation capability by developing a hybrid simulation approach using state-of-the-art Eulerian and Lagrangian methods for free-surface flow simulation.

RESULTS

In previous years of this project, we developed novel numerical methods for wind and wave motions; from simulations, the fundamental dynamics of wind-wave interactions were investigated. In FY 2009, we continued to investigate wind input to wave evolution and performed extensive analysis to connect our results to other studies. Figure 1 shows the dependence of wave-induced form drag on wave age $c/U_{\lambda/2}$. When the wave age is small, the form drag has a positive value, which results in growth of the water wave. As the wave age increases, the form drag increases first and reaches its peak value, and then decreases as the wave age further increases. The form drag vanishes around $c/U_{\lambda/2} = 1$, and becomes negative for large wave age, which results in wave attenuation. The simulation result obtained in this study is consistent with other simulation results in the literature, which are plotted in figure 1 for comparison.

Figure 2 shows the dependence of wave growth rate parameter β on the wave steepness ak for the slow wave case. As wave steepness increases, the growth rate parameter decreases. The measurement data compiled by Peirson & Garcia (2008) is also plotted for comparison. It is found that the result of the present study agrees well with the measurements in the literature.

Under the wind pressure forcing, the temporal growth rate of a water wave can be parameterized as $\gamma = S_{\lambda/2} (U_{\lambda/2}/c-1)| U_{\lambda/2}/c-1|$, where $S_{\lambda/2}$ is the sheltering coefficient. Based on laboratory measurement, Donelan (1999) obtained $S_{\lambda/2} = 0.28$. Donelan *et al.* (2006) further improved this parameterization by using wave-following field measurement data and showed that $S_{\lambda/2} = 0.17$. Figure 3 shows the comparison between our simulation result and the parameterizations. It is found that our simulation result agrees very well with the measurement and supports their improvement in the parameterization.

To investigate the interaction between wind turbulence and broadband wavefield, we performed a series of turbulence-wave coupled simulations. We constructed the initial wavefield based on the JONSWAP spectrum. Three cases with different wave ages based on the phase velocity at the peak wavenumber k_m, c_m/u^*=5, 12.3, and 16, are considered. Figure 4 shows the wave growth rate parameter β and the fractional rate of energy input γ as a function of wavenumber k for these three

cases. To help understand their behavior, we also plot the values of c/u* at different k for the three cases. Note that according to the wave dispersion relationship, c/u* decreases as k increases and has different ranges for the three cases. For the case of $c_m/u^*=5$, β reaches its peak around $k = k_m$ and decreases as k further increases. For the cases of $c_m/u^*=12.3$ and 16, β first increases with k and reaches its peak around $k = 2k_m \sim 3k_m$, and then decreases as k further increases. For all cases, β reduces significantly at large k (i.e., short waves in the spectrum); at these small scales, the pressure induced by the short waves is relatively small compared to the pressure fluctuation in the wind turbulence. On the other hand, γ, which measures the fractional rate of energy input to wave, does not reduce as rapidly compared to β (γ even increases with k for the case of $c_m/u^*=5$). In reality, local small waves may grow rapidly to break, serving as an important vehicle for atmosphere-ocean momentum and energy transfer.

We also extended our study to turbulence transport of scalars in the wind-wave field. Figure 5 shows the phase-averaged contours of the scalar concentration fluctuation root-mean-square (rms) value above water waves with wave ages c/u*=2 and 14. For the case of c/u*=2, the scalar fluctuation is high in the strong shear layer that starts from the wave crest to above the wave trough. For the case of c/u*=14, the high intensity region of scalar fluctuation is located above the windward face of the wave crest. This dependence of scalar fluctuations on the wave age is found to be similar to that of the streamwise velocity fluctuation.

For accurate estimation of the surface pressure in field measurement, it is necessary to put the pressure probe close to the wave surface. In figure 6, we compare the vertical pressure decay profiles of our slow wave cases to the Kudyavtsev *et al.* (2001) pressure profile shown by Donelan *et al.* (2006) with their record LG9. Two exponential profiles, exp(-kz) and exp(-0.55kz) are also plotted for comparison. The result shows that the pressure decay rate decreases as the wave steepness increases. When the measurement is taken at kz=0.2, the surface pressure values from our simulations collapse, and the two exponential extrapolations provide values with about 5% error; when the measurement is taken at kz=1 instead, the surface pressure values from different cases of our simulations diverge, and the extrapolations can have errors as large as 20%. This comparison confirms the advantage of wave-following pressure probe measurement.

Under high wind conditions, the wind-wave becomes steep and wave breaking may happen, which results in airflow separation and wave energy dissipation. Figure 7 shows the flow structures when instantaneous airflow separation happens over steep/breaking wind-wave. The enhanced airflow shear layer at the edge of the separation zone is clearly indicated by the high intensity of spanwise vorticity. The violent turbulence motion around the separation zone intensifies the turbulence mixing and momentum transport. Our analysis also shows that the strong reattachment of the airflow significantly increases the surface pressure and shear stress on the windward face of the preceding wave crest, and therefore enhances the form drag and tangential stress on the wave surface.

When wave breaking happens, the surface process becomes violent and full of small scale structures. In order to study the details of wave breaking as well as the associated airflow separation and spray droplet dynamics, we developed a novel hybrid simulation tool by coupling the strength of several multiphase fluid simulation methods. We use the coupled level-set and volume-of-fluid (CLSVOF) method to simulate the wind-wave interaction and the development of breaking wave at the full scale. Once wave breaking happens, locally a high resolution smoothed particle hydrodynamics (SPH) simulation is coupled with CLSVOF to resolve and track the violent motion of the fluid particles. Figure 8 shows an example of this CLSVOF-SPH coupled simulation.

IMPACT/APPLICATION

This project aims at a basic scientific understanding of the air-sea-wave interaction physics and numerical capability development for ocean wave-field prediction pertinent to Navy applications. It addresses a critical need of the Navy to bridge the gap between the modeling of small-scale air-sea-wave interaction physics and the prediction of ocean waves at regional scales. The proposed research will provide the Navy with a new powerful tool to predict deterministically nonlinear, large wavefield with finely-resolved temporal and spatial details. The new phase-resolved, deterministic tool is fundamentally distinct from existing phase-averaged, statistical wave modeling tools such as WAM and SWAN, with the potential of being able to make more accurate prediction because of its direct, physics-based approach. Furthermore, the results of this work will also be useful for the comparison and calibration of field measurements and for obtaining physical insights to improve existing phase-averaged wave prediction models.

RELATED PROJECTS

This work complements a number of on-going ONR projects. In particular, it is closely related to the development of Simulation of Nonlinear Ocean Wave-field (SNOW) by Professor Dick Yue's research group at MIT. The wind input and wave breaking dissipation modeling in this project is to be incorporated into SNOW, and together we will improve the SNOW capability for it to become a next generation of wave model capable of predicting nonlinear wave evolution subject to winds and whitecapping. Such numerical tools will be useful for high-resolution wave-field study.

REFERENCES

Banner, M. L. 1990 "The influence of wave breaking on the surface pressure distribution in wind-wave interactions," *J. Fluid Mech.* **211**, 463-495.

Banner, M. L. & Peirson, W. L. 1998 "Tangential stress beneath wind-driven air-water interface," *J. Fluid Mech.* **364**, 115-145.

Bole, J. B. 1967 "Response of gravity water waves to wind excitation," PhD thesis, Dept. of Civil Engineering, Stanford University.

Donelan, M. A. 1999 "Wind-induced growth and attenuation of laboratory waves," In *Wind-over-Wave Couplings: Perspectives and Prospects* (ed. S. G. Aajjadi, N. H. Thomas & J. C. R. Hunt), pp. 183-194. Clarendon.

Donelan, M. A., Babanin, A. V., Young, I. R. & Banner, M. L. 2006 "Wave-follower field measurements of the wind-input spectral function. Part II: Parameterization of the wind input," *J. Phys. Oceanogr.* **36**, 1672-1689.

Kihara, N., Hanazaki, H., Mizuya, T. & Ueda, H. 2007 "Relationship between airflow at the critical height and momentum transfer to the tranveling waves," *Phys. Fluids* **19**, 015102.

Kudryavtsev, V. N., Makin, V. K. & Meirink, J. F. 2001 "Simplified model of the air flow above the waves," *Boundary-Layer Meteorol.* **100**, 63-90.

Li, P. Y., Xu, D. & Taylor, P. A. 2000 “Numerical modelling of turbulent airflow over water waves,” *Boundary-Layer Meteorol.* **95**, 397-425.

Mastenbroek, C., Makin, V. K., Garat, M. H. & Giovanangeli, J. P. 1996 “Experimental evidence of the rapid distortion of turbulence in the air flow over water waves,” *J. Fluid Mech.* **318**, 273-302.

Peirson, W. & Garcia, A. W. 2008 “On the wind-induced growth of slow water waves of finite steepness,” *J. Fluid Mech.* **608**, 243-274.

Sullivan, P. P., McWilliams, J. C. & Moeng, C.-H. 2000 “Simulation of turbulent flow over idealized water waves,” *J. Fluid Mech.* **404**, 47-85.

HONORS/AWARDS/PRIZES

T. F. Ogilvie Young Investigator Lectureship
Invited to be a keynote speaker at the 2nd International Conference on Turbulence and Interaction

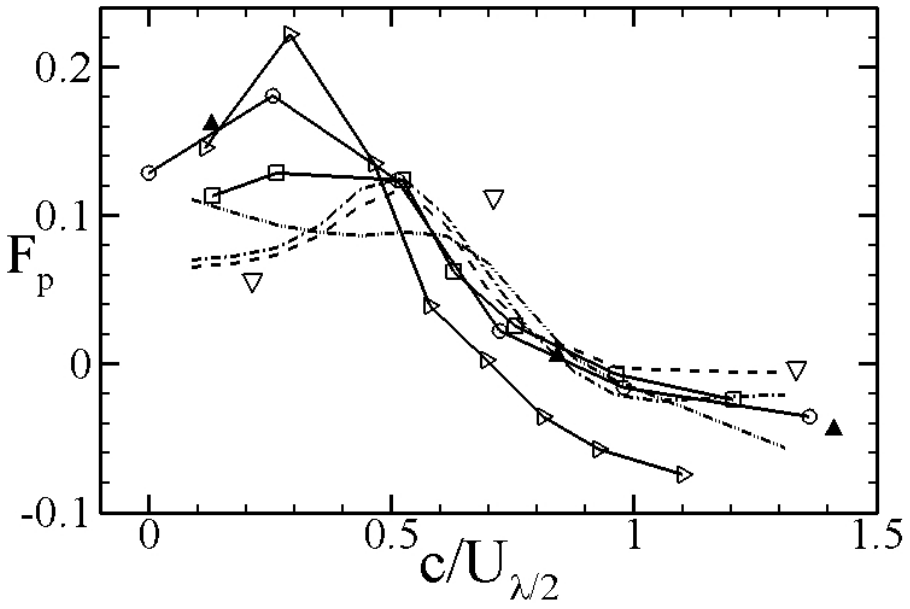

Figure 1. Wave-induced form drag F_p as a function of $c/U_{\lambda/2}$ for water wave with steepness ak=0.1. ◢, current DNS results ○, DNS results of Sullivan et al. (2000) □, DNS results of Kihara et al. (2007) ▽, results of Mastenbroek et al. (1996) with LRR closure. Results of Li et al. (2000) with different turbulent closure: —• —, E-κz; — ••—, q^2l; - - -, LRR.

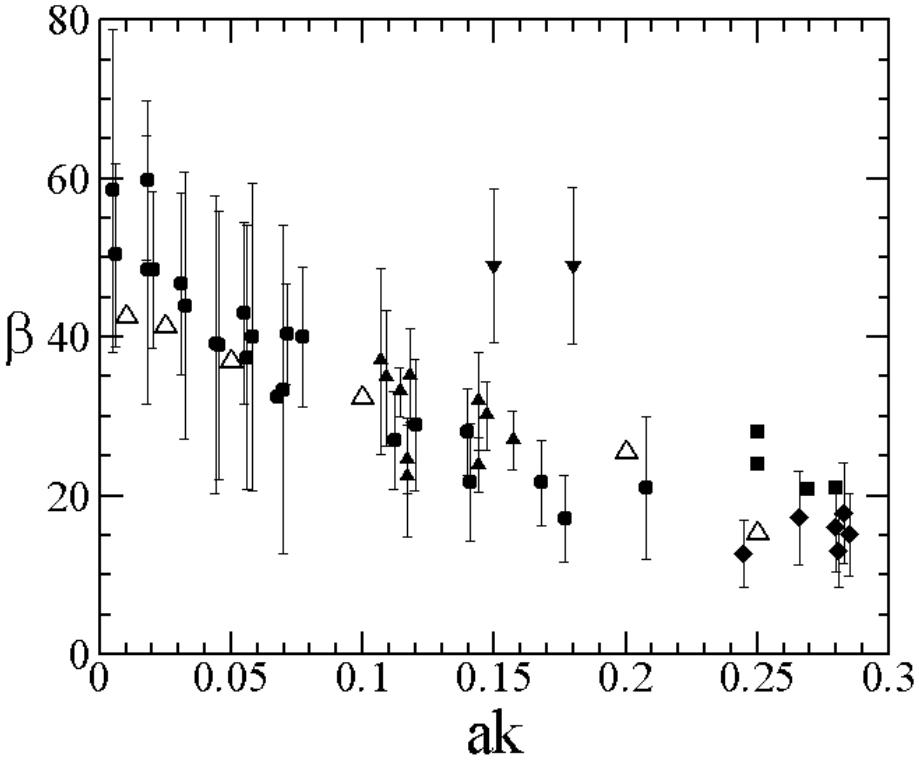

Figure 2. Wave growth rate parameter β for slow water waves plotted as a function of wave steepness ak. Measurement data compiled by Peirson & Garcia (2008) are denoted by solid symbols with error bars: ▲, Bole (1967); ■, Banner (1990); ▼, Mastenbroek et al. (1996); ◆, Banner & Peirson (1998); and ●, Peirson & Garcia (2008). Results of the present study are denoted by △.

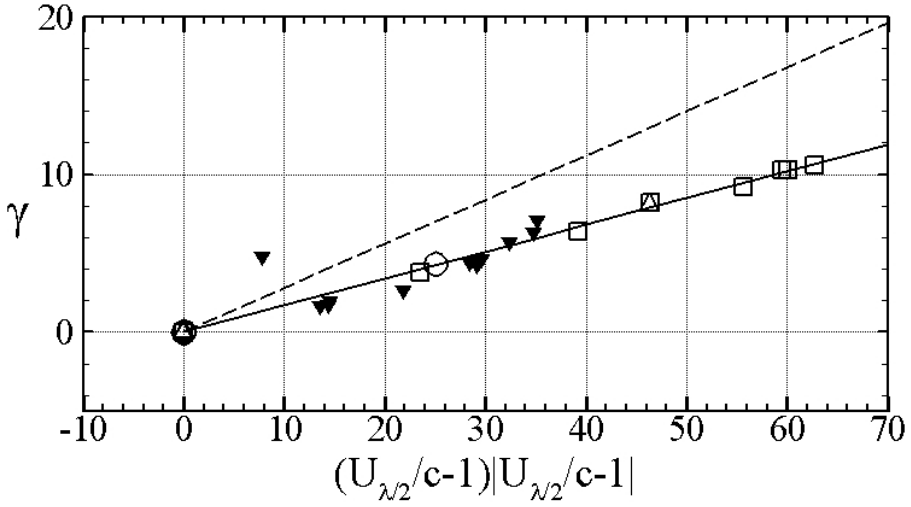

Figure 3. Comparison of temporal growth rate γ with Donelan et al. (2006): —, their parameterization γ=0.17(U λ/2/c-1)\| U λ/2/c-1\|; ◤, their hindcast estimates based on the data of Donelan (1999); - - -, parameterization of Donelan (1999) γ=0.28(U λ/2/c-1)\| U λ/2/c-1\|. Results of current simulation are denoted by open symbols: □, Airy wave with various steepness; △, Airy wave with steepness ak=0.25; ○, Stokes wave with ak=0.25.

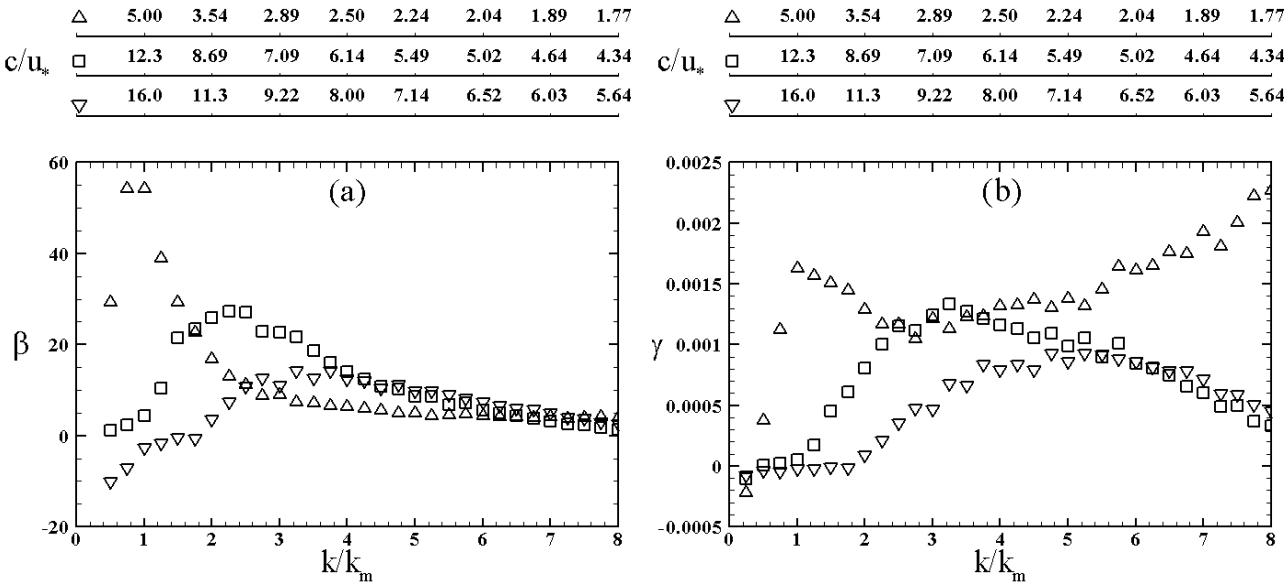

Figure 4. (a) Wave growth rate parameter β, and (b) fractional rate of energy input γ, for three broadband wave cases: △, $c_m/u^*=5$; □, $c_m/u^*=12.3$; and ▽, $c_m/u^*=16$.

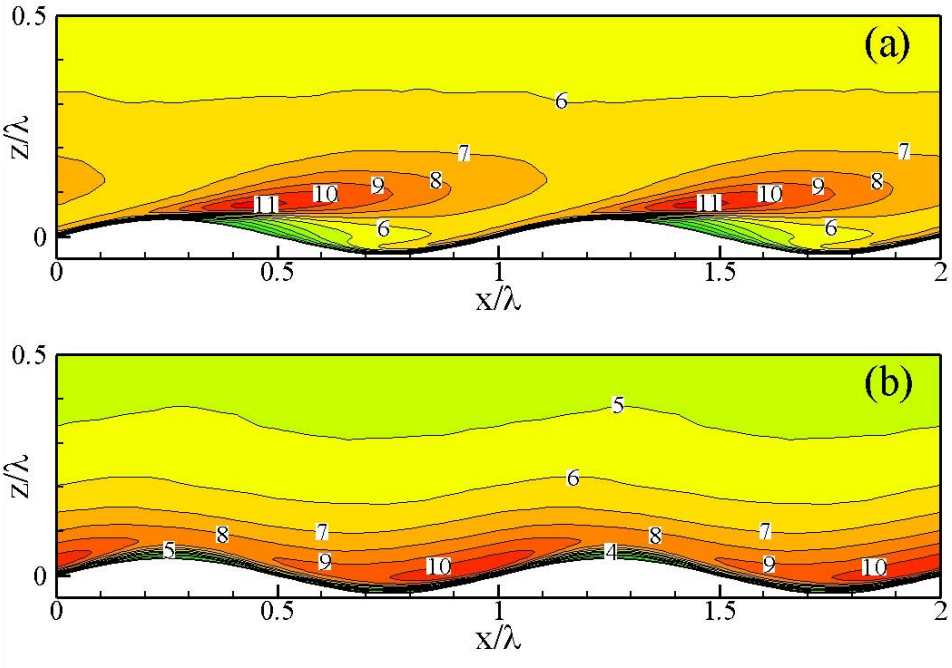

Figure 5. Contours of phase-averaged scalar fluctuation rms above water waves with steepness ak=0.25 and wave ages: (a) c/u*=2; and (b) c/u*=14. The surface wave propagates in the +x-direction.

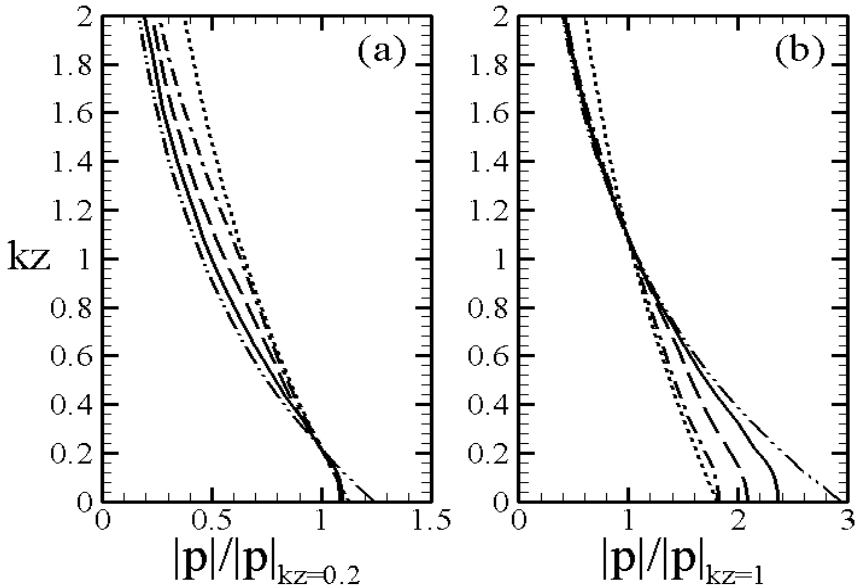

Figure 6. Comparison of pressure profiles with exponential decays: solid line, the Kudryavtsev et al. (2001) profile estimated by Donelan et al. (2006) with steepness ak=0.05 and wave age c/u*=3.5 (their record LG9); dashed line, present result for water wave with (ak, c/u*) = (0.1, 2); dash-dot line, the present result for water wave with (ak, c/u*) = (0.25, 2); dash-dot-dot line, exponentially decay with exp(-kz); dotted line, exponentially decay with exp(-0.55kz). The profiles are normalized by the pressure amplitude |p| at (a) kz=0.2 and (b) kz=1, respectively (i.e., assuming that the measurements are conducted at the corresponding heights).

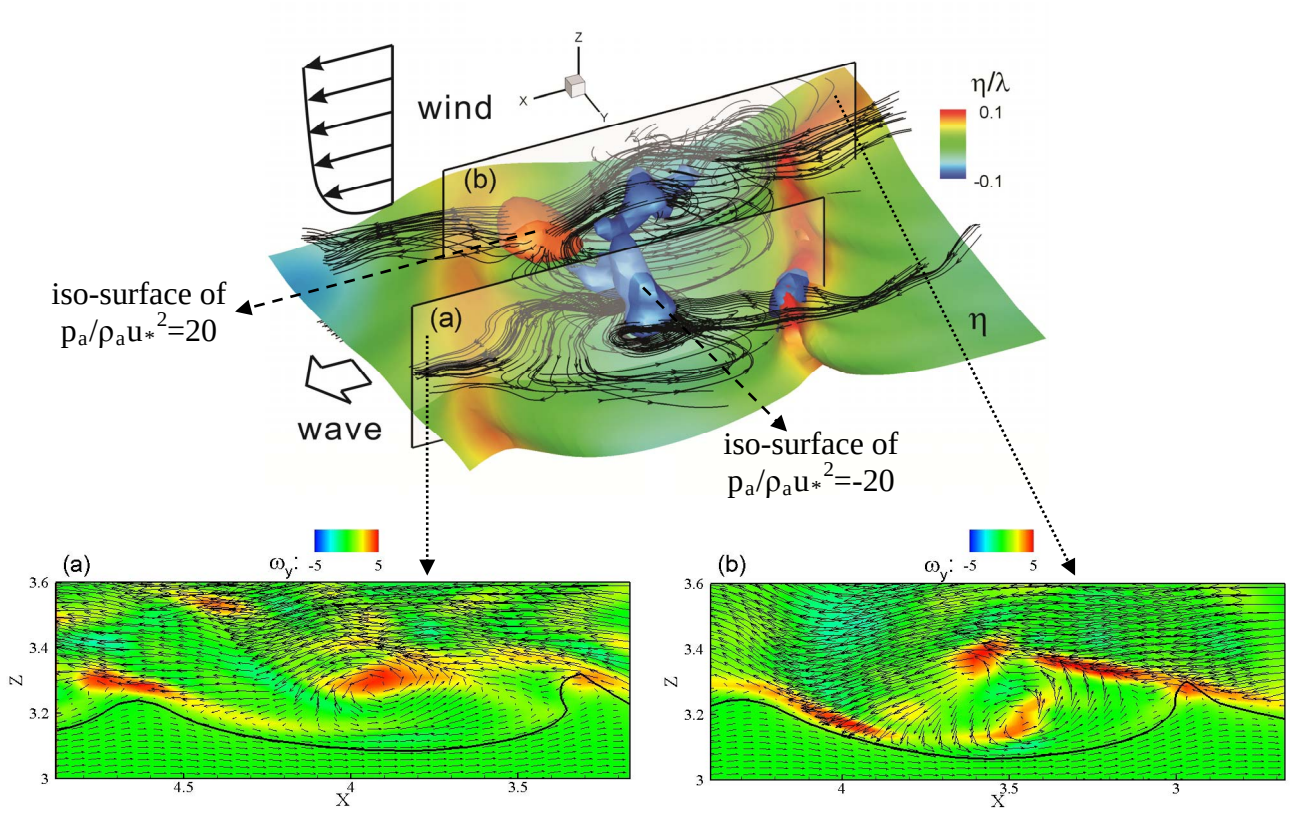

Figure 7. Instantaneous airflow separation over a steep wave prior to breaking under high wind condition with two different reattachment condition on the windward face of the preceding wave crest: (a) weak reattachment, and (b) strong reattachment. The instantaneous three-dimensional velocity vectors are projected and plotted on a (x; z)-plane crossing the center of the separation zone. The flow fields are plotted in a frame following the wave crest. The strong shear layers at the edge of the separation bubble and near the reattachment point are indicated by the high intensity of spanwise vorticity.

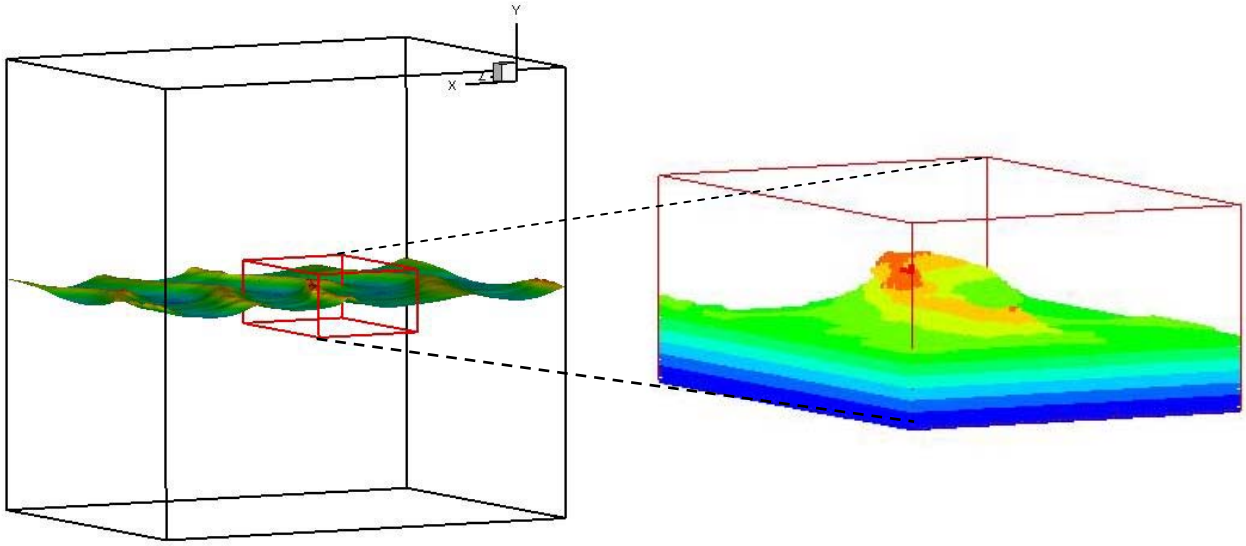

Full scale Eulerian simulation using coupled level-set and volume-of-fluid method

Local scale high resolution Lagrangian simulation using smoothed particle hydrodynamics

Figure 8. CLSVOF and SPH coupled simulation.